Geomechanics and Engineering, *Vol. 17, No. 5 (2019) 429-438*
DOI: https://doi.org/10.12989/gae.2019.17.5.429

Debonding of microbially induced carbonate precipitation-stabilized sand by shearing and erosion

Jinung Do[a], Brina M. Montoya* and Mohammed A. Gabr[b]

Department of Civil, Construction, and Environmental Engineering,
North Carolina State University, 2501 Stinson Drive, Raleigh, NC 27607, U.S.A.

(Received October 10, 2018, Revised February 4, 2019, Accepted February 5, 2019)

Abstract. Microbially induced carbonate precipitation (MICP) is an innovative soil improvement approach utilizing metabolic activity of microbes to hydrolyze urea. In this paper, the shear response and the erodibility of MICP-treated sand under axial compression and submerged impinging jet were evaluated at a low confining stress range. Loose, poorly graded silica sand was used in testing. Specimens were cemented at low confining stresses until target shear wave velocities were achieved. Results indicated that the erodibility parameters of cemented specimens showed an increase in the critical shear stress by up to three orders of magnitude, while the erodibility coefficient decreased by up to four orders of magnitude. Such a trend was observed to be dependent on the level of cementation. The treated sand showed dilative behavior while the untreated sands showed contractive behavior. The shear modulus as a function of strain level, based on monitored shear wave velocity, indicated mineral debonding may commence at 0.05% axial strain. The peak strength was enhanced in terms of emerging cohesion parameter based on utilizing the Mohr-Coulomb failure criteria.

Keywords: microbially induced carbonate precipitation (MICP); bio-cementation; triaxial testing; impinging jet testing; erodibility

1. Introduction

Microbially induced carbonate precipitation (MICP) is a novel approach for improving soil strength and modulus by harnessing natural microbial communities to catalyze carbonate-based precipitation. Urea is easily dissolved in water, however, it is not ionized due to the hydrogen bonding between urea and water molecules. Urease enzymes in ureolytic bacteria, however, can hydrolyze the urea through the metabolic activity of the microbes, thus producing carbonate ions. With the presence of calcium, a natural bonding agent, calcium carbonation is precipitated, per the reaction shown in Eq. (1)

$$CO(NH_2)_2 + 2H_2O - urease\ enzyme \rightarrow 2NH_4^+ + CO_3^{2-}$$
$$Ca^{2+} + CO_3^{2-} \rightarrow CaCO_3 \downarrow \tag{1}$$

Stock-Fischer *et al.* (1999) proposed the key principles of the MICP process, and DeJong *et al.* (2006) showed the applicability of MICP from a geotechnical perspective. Since then, the MICP process has gained wide interest (Montoya 2018) including physical aspects (e.g., mechanical behavior, particle detachment, hydraulic conductivity), biochemical aspects (e.g., effect of salinity, pH, kinetics), and modeling (e.g., mathematical, reactive transport, geomechanical) as presented by Montoya and DeJong (2015), Salifu *et al.* (2016), Sidik *et al.* (2014), Cheng *et al.* (2014), Putra *et al.* (2017), Ferris *et al.* (2003), van Wijngaarden *et al.* (2011), Nassar *et al.* (2018), among many others.

A key soil improvement application of MICP is to strengthen soil against the occurrence of scour adjacent to foundation systems. When flow in streams, currents, and waves approaches the foundation elements, turbulent flow occurs around the system inducing shear stress on the soil surface. These stresses cause soil to scour, undermining the support of the foundation elements and, therefore, the potential for structural failure. There are more than 600,000 bridges in the United States, and over 80 percent of the bridges are over water (NBI 2016). Briaud (2006) reported that 60 percent of the bridge failures from 1966 to 2005 are associated with hydraulic causes, especially scour of foundation soil. In addition, the anchoring and mooring systems of a broad range of offshore structures represent a major component of the installation costs. This is especially true when scour is a concern. Therefore, scour mitigation is a critical step for assessing the stability of foundation systems over water during design and post construction stages as well as throughout the support system operational life.

There are traditionally two mitigation approaches for scour issues. A static mitigation measure which seeks to place a rock armor, or similar armor material, around the foundation elements. This approach requires the careful design of filter layers below the armors to minimize the sinking of the rock layer into the bed sediments. This method is costly as it calls for the transportation and placement of the rock materials in a commonly dynamic

*Corresponding author, Assistant Professor
E-mail: bmmorten@ncsu.edu
[a]Ph.D. Candidate
[b]Distinguished Professor

ISSN: 2005-307X (Print), 2092-6219 (Online)

flow environment. In addition to the risk of having the rock layer sink into the soft seabed sediments, a portion of the rock material might be washed away if placement takes place in high-speed current environment. A second approach is referred to as a dynamic approach where the scour hole is first allowed to fully develop, and then the hole is filled with rock armor. To use this approach, however, a superstructure could not be deployed until the scour hole has developed and backfilled with the rock material. This poses uncertainty regarding the time to reach scour depth equilibrium. There is no assurance that scour will not occur at the edges of the filled scour pit and still lead to reduced foundation capacity. In addition to the uncertainty with time to installation, this is also a costly approach since mobilization of construction equipment is needed several times during the construction phase.

On the other hand, stabilization of sand using MICP may provide an alternative solution for scour mitigation. The idea is to bio-mediate the soft soil around the foundation system in a zone that extends (laterally and with depth) 2~5 times the diameter of the area of concern. This geometry covers an equivalent soil mass normally susceptible to scour. Such geometry in terms of depth and lateral extent, for example, is necessary to ascertain the lateral capacity of pile foundation. The successful development of MICP process for scour mitigation will lead to less frequent maintenance and extends the economic life-cycle cost of the deployed foundation system. MICP can be initiated by augmenting exogenous bacteria or by stimulating indigenous bacteria (Gomez *et al.* 2016). Therefore, MICP technology is potentially suitable for enhancing the loose sediment's scour resistance under submerged conditions where the implementation of conventional methods can be challenging.

Several researchers have focused on the mechanical behavior of MICP-treated soils. Lin *et al.* (2015) and Feng and Montoya (2015) observed the shear responses of treated sands under axial compression at the confining stress range of 25 kPa to 100 kPa and 100 kPa to 400 kPa, respectively. Lin *et al.* (2015) indicated that the cohesion of MICP-treated sand improved with no discernable increase in the friction angle. Feng and Montoya (2015) presented the improvement of the fiction angle with insignificant increase in the cohesion parameter for a range of stresses for which the failure envelope was observed to be linear rather than curved. In addition, the commencement of bonding breakage occurs before reaching the peak stress level on the stress-strain relationship (Feng *et al.* 2017).

On the other hand, Maleki *et al.* (2015) and Zhan *et al.* (2016) demonstrated the high resistance of MICP-treated soils to wind-induced erosion for fugitive dust control. Jiang *et al.* (2016) induced the internal erosion of MICP-treated sand-clay mixtures through seepage and derived erosion-related parameters (e.g., peak erosion rate, erosion coefficient) for given levels of cementation.

In this paper, the erodibility and the shear response of MICP-treated sand under submerged impinging jet and axial compression, respectively, were evaluated to understand the shear strength behavior and erosion potential of MICP-treated sand at low confining stresses. The scope presented herein includes triaxial testing, submerged impinging jet (mini JET apparatus) testing, and microscale analysis on uncemented and MICP-cemented sand specimens.

2. Materials and methods

2.1 Test soil

A test sand from a local quarry (*X-FINE SAND,* 99.72% of Silica, *Southern Products & Silica Company*, *Inc*., Hoffman, NC) was used. The sand has a specific gravity (G_s) of 2.66, a mean particle size (D_{50}) of 0.49 mm, a minimum and maximum void ratio ($e_{\min}$ and $e_{\max}$) of 0.61 and 0.91, respectively, and was classified as a poorly graded sands (*SP*) under the Unified Soil Classification System (USCS). The specimens for testing were prepared by air pluviation to a relative density of approximately 30%.

2.2 Triaxial testing

The shear response of the MICP-treated sand was evaluated using drained triaxial compression (Fig. 1(a)). The targeted dimensions of the specimen were 72 mm in diameter and 144 mm in height. The effective overburden stress within the depth prone to scour ranges from 0~60 kPa, assuming the submerged soil's unit weight of approximately 10 kN/m^3 (e.g., 20 kN/m^3-9.81 kN/m^3) and a maximum scour depth of 6 m (twice the pile diameter equal (Richardson *et al.* 1991)). Three levels of confining pressure were needed to ascertain the strength parameters. Therefore, effective confinement stresses of 10 kPa, 30 kPa, and 50 kPa were used to represent relevant in situ stress levels. Each test sample was saturated before biological inoculation, and then treated while vented to prevent the specimen from desaturating by gas released during the ureolytic process. Once the specimen reached the target level of cementation, the specimen was fully saturated by back pressure until the *B*-value was over 0.95. Due to the focus on the calcium carbonate precipitation process, CO_2 was not used to facilitate the saturation phase. Instead, high levels of back pressures (e.g., 200~400 kPa) were applied for a longer period of time (e.g., up to two weeks) until the target *B*-value was achieved. Finally, the axial compression under drained conditions was applied until 12% axial strain was reached.

(a) Triaxial testing (b) Mini JET apparatus

Fig. 1 Testing devices

The MICP process was monitored during the treatment process by measuring the shear wave velocity using bender element sensors installed within the triaxial sample end caps. A stainless steel wire was inserted at the receiving bender element to reduce electrical crosstalk in the received signal (Montoya *et al.* 2012). A 10 V sinusoidal wave with 10 kHz frequency was generated by a function generator (*Agilent 33522A*) and received by a digital oscilloscope (*Agilent MSO6014A*). The pre-measured tip-to-tip distance was divided by the first arrival time of the propagated signal to calculate the shear wave velocity of the specimens. Montoya and DeJong (2015) proposed three representative shear wave velocities at 1 atmospheric pressure to distinguish the various levels of cementation based on the site classification defined by NEHRP (2003). Three values were selected as target levels of cementation: 400 m/s for lightly, 700 m/s for moderately, and 1200 m/s for heavily cemented soil.

2.3 Submerged impinging jet testing

A submerged impinging jet testing device, mini JET apparatus, with a 101.6 mm diameter and 116.4 mm height was used to assess the erodibility of the treated specimens (Fig. 1(b)). Each test specimen was treated under 50 kPa of effective overburden pressure. During the mini JET testing, the surface of the test material was subjected to erosion by a jet induced via a constant differential head. The applied shear stress (τ_i) is calculated as a function of the pressure head (h), the nozzle diameter (d_0), and distance between the jet orifice and the surface of material (J_i+s) as shown in Eq. (2) (Al-Madhhachi *et al.* 2013)

$$\tau_i = C_f \rho_w \left(C\sqrt{2gh}\right)^2 \left(\frac{C_d d_0}{J_i + s}\right)^2 \tag{2}$$

where, C_f is a coefficient of friction = 0.00416, ρ_w is a fluid density = 1000 kg/m^3, C is a coefficient of discharge measured, g is a gravitational acceleration, C_d is a diffusion constant = 6.3, J_i is an initial distance between the nozzle and un-deformed soil surface, and s is a scoured depth due to the induced impinging jet. The potential energy due to established head differential (h) causes a shear velocity at the nozzle ($C\sqrt{2gh}$) providing a shear stress at the nozzle ($C_f \times \rho_w (C\sqrt{2gh})^2$). The applied shear stress at the nozzle is converted to an applied shear stress at soil surface using the relationship with the nozzle diameter (d_0) and the distance between the nozzle and soil surface (J_i+s) as given by Eq. (2).

During testing, the head differential (h) was increased until the scour was initiated. The value of h usually increased from 0.1 m (τ_i≈0.1 Pa) to 5 m (τ_i≈90 Pa) until the scour was observed. Once the scour was initiated, the scoured depth and corresponding time were recorded until no more scour occurs under the constant pressure. At this equilibrium state, the applied shear stress is called a critical shear stress (τ_c). The detailed of the testing procedures are described by Khanal *et al.* (2016).

A linear erosion model with erodibility parameters including critical shear stress and erodibility coefficient was used to quantify the detachment process of the test sand. The induced erosion rate (ε_r) is expressed per Eq. (3)

$$\varepsilon_r = k_d(\tau_i - \tau_c)^\alpha \tag{3}$$

where, ε_r is an erosion rate, k_d is a erodibility coefficient, and α is an exponent usually assumed to be unity for sandy soils (Hanson and Cook 2004). ε_r and τ_i are erosion variables, while k_d and τ_c are called erodibility parameters. Thus, τ_c was calculated where J_i+s reaches equilibrium, then using τ_i and ε_r, k_d was derived with the calculated τ_c assuming α=1. To monitor the improvement of shear wave velocity of the specimens, bender elements were attached at the top and bottom caps of the specimens used for scour testing, in a manner similar to the triaxial setup.

2.4 Treatment

Sporosarcina pasteurii (American Type Culture Collection (ATCC) 11859) was incubated in a growth media (ATCC 1376) at 200 rpm and 30 °C until the optical density at a wavelength of 600 nm, OD_{600}, was approximately 1.0. Two pore volumes of the bacterial inoculant (e.g., 0.333 M of urea, 0.374 M of NH_4Cl, and 15 ml/100 ml bacterial suspension, as presented by Feng and Montoya 2015) were introduced into specimens with the seepage velocity of 0.0091 cm/sec. After 6 hours retention, the cementation solution composed of 0.333 M of urea, 0.374 M of NH_4Cl, and 0.05 M of $CaCl_2$ was injected at intervals of 6, 6, and 12 hours until the target shear wave velocity was achieved. Once the targeted cementation level was achieved, the treated specimens were flushed with water to eliminate further reactions inside the specimen.

2.5 Assessment

Before and after treatment, constant head tests were conducted to evaluate the hydraulic conductivity of the specimens. After the completion of the triaxial testing, each sheared specimen was returned to its original height. The remolded specimen was divided into 7 segments of approximately 2 cm each. The segments were then washed using 1 M hydrogen chloride to quantify the distribution of the precipitated calcium carbonate. In case of the impinging jet system, the specimen was extracted from the mold after testing, and the mass of calcium carbonate was measured in the same manner applied to the triaxial specimens. The mass of calcium carbonate was expressed in percent as the ratio of the mass of calcium carbonate over the mass of the untreated soil gravimetrically. Then the erodibility parameters were correlated as a function of the level of cementation.

The shear wave velocity (V_s) was assessed as a function of the strain during the shearing phase of the triaxial testing. The strength parameters (friction angle and cohesion) were derived on the basis of the Mohr-Coulomb failure criterion. Based on the derived strength parameters, the stress-dilatancy relation of treated sand was evaluated according to the model presented by Zhang and Salgado (2010).

Microscopic analyses were used to understand the morphological and elemental characteristics of the cemented particles using variable pressure scanning electron microscopy (VP-SEM, *Hitachi S3200N*) and energy-dispersive X-ray spectroscopy (EDS, *Oxford*

Instruments X-Max) with a beam accelerating voltage of 20 kV and a beam current of 80 nAmps. Samples were coated with 42 nm of gold-palladium (60% of Au and 40% of Pd) prior to the scanning. The X-ray energy was analyzed by *Aztec* (*Oxford Instrument*).

3. Results

3.1 Detachment behavior

The improvement of the shear wave velocity as a function of the number of injections is shown in Fig. 2. Three lightly, three moderately, and two heavily cemented specimens were treated to evaluate the erosion resistance as a function of cementation level. After flushing the specimen with water and measuring the hydraulic conductivity, the impinging jet erosion testing was conducted on specimens with various levels of cementation. Data in Fig. 3 include the applied shear stress calculated by Eq. (2) once the scour was initiated. In this case, the untreated specimen was scoured rapidly and an ultimate scour depth was reached within one minute under the lowest applied shear stress (0.16 Pa). The MICP-treated specimens, however, tolerated higher applied shear stresses with lower scour magnitude. In addition, the time to reach the ultimate scour depth increases, in general, with the level of cementation (e.g., moderately and heavily cemented ones).

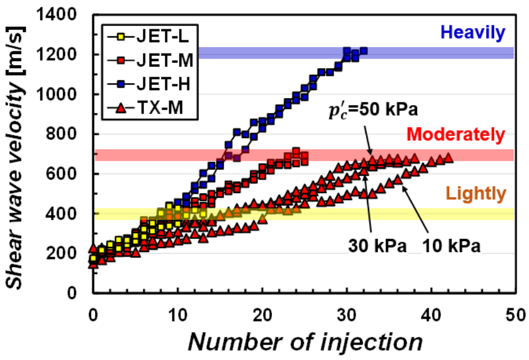

Fig. 2 Improvement of specimens' shear wave velocity during treatment. Triangular symbols indicate triaxial specimens (TX), rectangular symbols represent mini JET specimens (JET); 'L' as lightly (V_s≈400 m/s), 'M' as moderately (V_s≈700 m/s), and 'H' as heavily cemented (V_s≈1200 m/s)

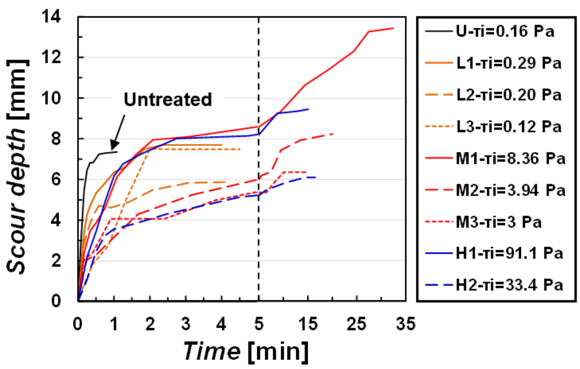

Fig. 3 Results of mini JET testing with diversely cemented specimens

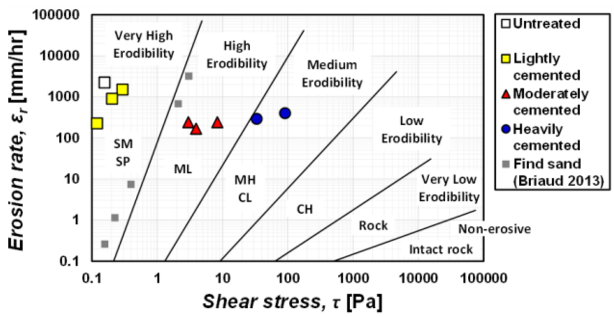

Fig. 4 Initial erosion rate-initial shear stress relationship with erodibility chart proposed by Briaud (2013)

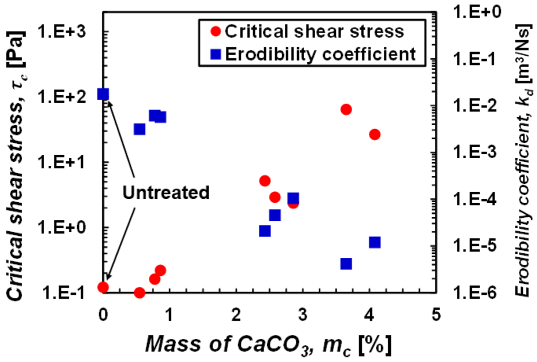

Fig. 5 Correlation with respect to the erodibility parameters and level of cementation

Briaud (2013) proposed an erodibility chart based on the applied shear stress and the erosion rate for different geomaterials. The initial applied shear stress after the occurrence of scour and the corresponding initial erosion rate are plotted on the erodibility chart (Fig. 4). The untreated and lightly cemented specimens show an erodibility level equivalent to that of sand, while the moderately and heavily stabilized sand specimens show erodibility levels equivalent to that of low to high plastic silts and lean clay.

The relationship between the scour depth and time is merely dependent on the level of the applied shear stress. Data in Fig. 5 represent the correlation between erodibility parameters calculated by Eqs. (2) and (3) and the level of cementation. The derived erodibility parameters were correlated with the relevant mass of calcium carbonate (i.e., at top segment of the specimen) as the erosion during testing occurs mainly at and near the surface. The critical shear stress values are improved up to three orders of magnitude, while the corresponding erodibility coefficients are reduced by nearly four orders of magnitude compared to the unstabilized specimen. Therefore, it seems at least m_c=2% (e.g., moderate levels of cementation) may be needed to increase the resistance of sand against erosion. Thus, as moderately treated specimens showed a threshold cementation level for the improvement in erosion resistance, three specimens with moderate level of cementation were prepared to assess the potential improvement in shear strength.

3.2 Shear response

The improvement of the shear wave velocity during the

(a) Untreated specimen (b) Treated specimen

Fig. 6 Different failure modes after shearing under 50 kPa confining stress

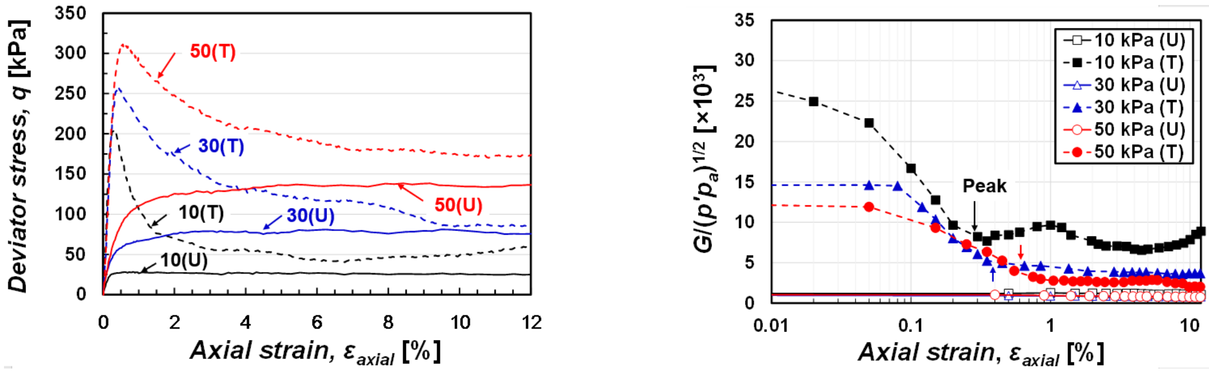

(a) Stress-strain relationship (b) Normalized shear modulus-strain relationship

Fig. 7 Results of triaxial testing with denoted values as the confines stresses, '*U*' as untreated and '*T*' as treated sands

treatment of the triaxial testing specimens are shown in Fig. 2. As the shear wave velocity is a function of the confining stress, different number of injections were observed to achieve the similar target shear wave velocities of the various specimens.

The untreated and treated specimens were sheared and showed different failure modes as shown in Fig. 6. The untreated specimen showed a bulging mode at 12% axial strain (Fig. 6(a)), while clear shear bands were observed for the treated specimen (Fig. 6(b)). Thus, the failure mode changes from ductile to brittle failure as the calcite precipitation is achieved. Interestingly, two shear bands were observed for the treated specimen as a secondary shear band was generated after the occurrence of the primary shear band. Feng *et al.* (2017) explains the shear band of MICP-treated sands occur due to the densification from precipitation. It is possible that cumulative densification during shearing induces secondary shear band in association with the dilative behavior.

The relationship between the stress and strain and the changes in the shear stiffness of untreated and treated sands under axial compression are shown in Fig. 7. All unstabilized specimens (solid lines in Fig. 7(a)) show hardening until around 2% axial strain and converged to plateau stress level which is representative of specimens tested in a loose state. The MICP-stabilized specimens (dotted lines in Fig. 7(a)), however, show a rapid increase in the deviatoric stress at the beginning of shearing to a peak strength, and then soften in a manner similar to dilative soils. The volumetric strain supports the dilative behavior as the volumetric strain range for untreated sands is 1.8~2.7%, while those for treated sands are 4.6~6% as positive volumetric strains are dilative. Due to the same level of stiffness (i.e., V_s), the initial slopes of the stress-strain relationship of treated sands are similar prior to the peak point. Not only the peak stress of the specimens, but also the residual stresses of MICP-treated sands is higher than the ultimate stress of the untreated sands.

The measured shear wave velocity was normalized with respect to the confining stress ($\rho V_s^2/[p'\cdot p_a]^{1/2}=G/[p'\cdot p_a]^{1/2}$; ρ: soil density, p': mean effective principal stress, p_a: atmospheric pressure, G: shear modulus). Such presentation meant to normalize the results with respect to the effect of increasing confining stress, so that the debonding process of the cemented sands with the progress of shearing can bemore clearly evaluated. Fig. 7(b) shows an indication of the possible macroscale debonding of MICP-treated sands under shearing with increase in axial strain. The normalized shear modulus of unstabilized specimens remains nearly constant over the strains range (e.g., $G/[p'\cdot p_a]^{1/2}$=1500). On the other hand, the normalized shear modulus of bio-treated specimens show a significant drop in the normalized shear modulus starting at approximately 0.1% axial strain, while the peak stresses are observed later at 0.3% strain. This observation implies that the onset of macroscale debonding occurs at strain (0.05~0.1%) causing the global yielding at 0.5~1% strain. After reaching the peak strength, the shear stiffness remains roughly constant; therefore, most

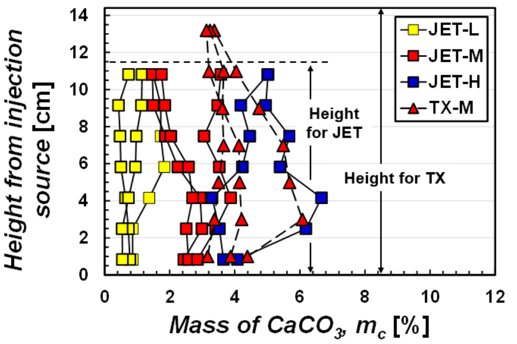

Fig. 8 Precipitation profile of mini JET and triaxial testing

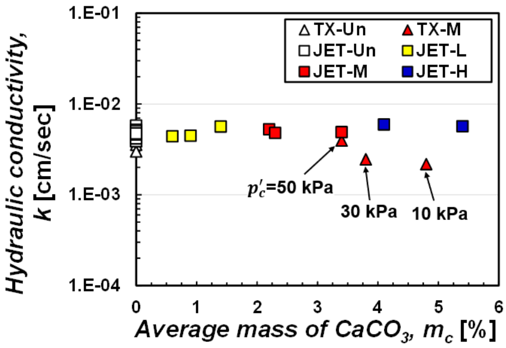

Fig. 9 Hydraulic conductivities before and after treatment

debonding effect on the normalized shear modulus of the MICP-treated sands takes place before observing the peak strength.

3.3 Distribution of cementation

The mass of calcium carbonate (m_c) as a function of the height of the specimen is shown in Fig. 8. The results show that the patterns of cementation distribution are not identical for similar target shear wave velocities. The precipitated profile is affected by the distribution of bacteria, the direction of flow, and the number of treatment. Non-uniformity of the profile seems to increase with increasing number of treatments. While high m_c is expected at the source of the injection, the precipitated crystals begin to transport further from the location of the injection following the direction of flow, as was observed Martinez *et al.* (2014). The applied hydraulic gradient influences the distribution of the precipitated minerals as well because the induced seepage forces transport the nucleate crystals to further locations along the direction of the flow before fixation on the particles occurs (Martinez *et al.* 2014).

The calcium carbonate distribution over the whole specimen influences the shear response of the specimen because the load is transferred throughout the domain globally. However, in the case of erosion potential, and during the impinging jet testing, the m_c for the top part near surface of the specimen is the most influential because the diffusion of the jet is mainly applied on the surface of the treated specimen.

3.4 Hydraulic conductivity

The hydraulic conductivities of untreated and treated specimens were measured. The magnitude of the hydraulic conductivity is related to the potential for dissipation of induced pore pressure, and consequently affects shear response and detachment process (Fig. 9). An average mass of calcium carbonate throughout the height was used to correlate with the measured hydraulic conductivity. Even after the cementation has occurred, the hydraulic conductivity did not seem to change significantly. The hydraulic conductivities of the specimens confined isotropically (i.e., TX) decreased by approximately 50% as the confinement stress is lowered. Since the shear wave velocity is a function of the confining stress, more cementation is required to achieve the same level of shear wave velocity compared to specimens confined at higher stresses (Fig. 2); the higher stress level can cause higher reduction of the hydraulic conductivity. In case of mini JET setup, the hydraulic conductivity shows approximately 25% variations. Different mechanism of the flow under different confining stress could affect the change in the hydraulic conductivity values of the treated sand.

Garcia-Bengochea and Lovell (1981) established that the hydraulic conductivity is highly governed by flow through the relatively larger sized pores. Recent research by Dadda *et al.* (2018) revealed cases for which calcium carbonate precipitation during the MICP process is mostly localized at the particles' contact points rather than uniformly distributed along the particle surface. It is therefore likely that the nature of change in k with the introduction of the MICP process is not unique but rather is a function of the treatment protocol leading to the cementation. It seems that there is a threshold level of precipitation that is needed to induce the reduction of the hydraulic conductivity. On the other hand, if the large-size pores are not impacted by the precipitation process, fluid flows preferentially through less cemented area; it is reasonable to anticipate slight change in the hydraulic conductivity.

3.5 Microscopic analysis

A stabilized specimen under 10 kPa confinement was collected after triaxial testing and used for SEM (Fig. 10) and EDS (Fig. 11) to analyze the precipitated morphology and constituents. As shown in Fig. 10(b), MICP generally occurs at the particle contacts as well as the particle surfaces (DeJong *et al.* 2010). The cementation at particle contacts primarily attribute to the peak shear strength and shear stiffness. The precipitation at the particle surfaces

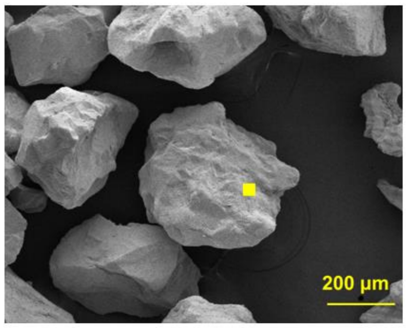

(a) Untreated sands

Fig. 10 SEM images

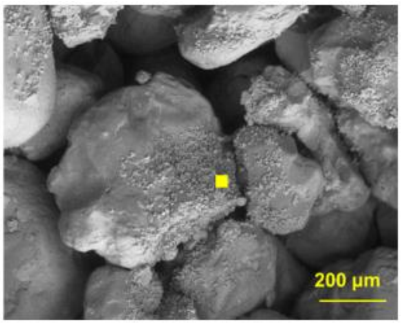

(b) Treated sands

Fig. 10 Continued

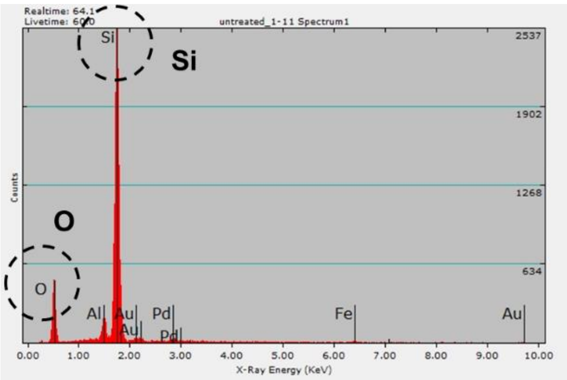

(a) Untreated sands

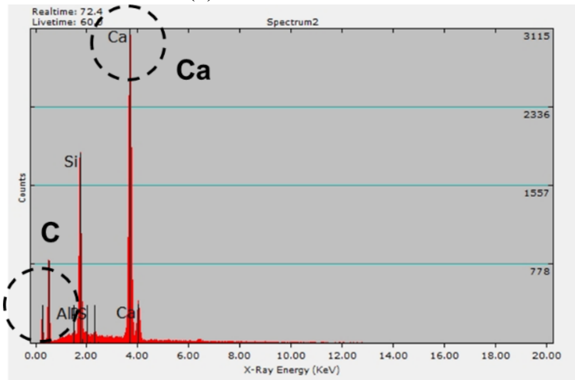

(b) Treated sands

Fig. 11 EDS results

attributes to the residual strength (Kim and Park 2017, Bolton 1986). The EDS results support the evidence of the cementation induced by MICP as the calcium and the carbon are observed in Fig. 11(b) is compared to Fig. 11(a) in which mainly silica is shown.

4. Discussion

4.1 Strength parameters depending on stress range

Based on the peak strength and the stress-strain relationship, the Mohr-Coulomb failure envelop is shown in Fig. 12. The strength was improved by exhibiting an increase in the cohesion (c) with cementation (e.g., an increase in cohesion from 0 kPa to 46 kPa) while the friction angle (e.g., a friction angle of 35º) remained constant assuming a linear Mohr-Coulomb failure envelop over the testing stress range. This enhancement is similar to observation on synthetically cemented and biopolymer treated sands by Clough *et al.* (1981) and Qureshi *et al.* (2017), respectively.

It is important to note that the failure envelop varies according to the level of confinement as summarized in Table 1. Results presented in Table 1 are from the moderately cemented specimens (e.g., V_s≈600-800 m/s). Data at the low confinement in this study and Lin *et al.* (2015) show the improvement in shear strength from MICP results to include a change in the cohesion parameter from 0 kPa to 50 kPa and 58 kPa, respectively, while the friction parameter remains relatively constant (Table 1). In constrast, at higher confinement, the main improvement in shear strength was captured as an increase in friction angle with a small increase in the cohesion parameter (Feng and Montoya 2015). Recent research by Nafisi *et al.* (2019) observed the shear strength envelopes of bio-cemented sands are nonlinear depending on the range of effective confinement. This suggests that there may be a transitional stress range where the nature of improvement in shear

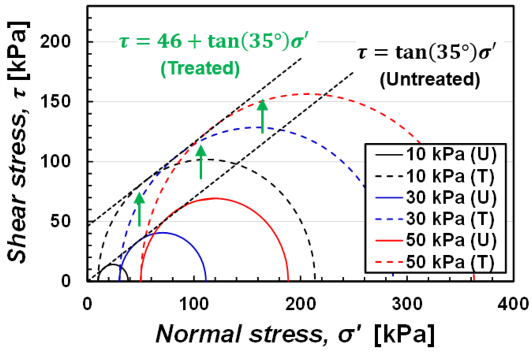

Fig. 12 Mohr-Coulomb failure envelope on untreated and treated sands based on peak stress

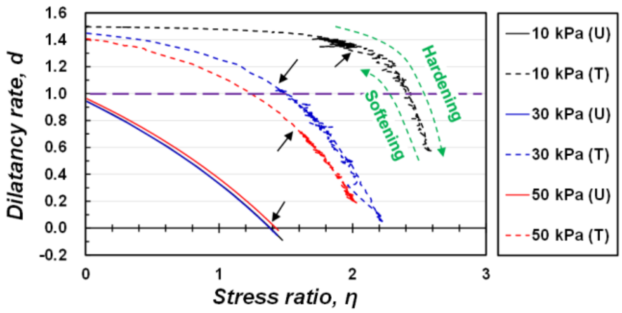

Fig. 13 Dilatancy tendency on untreated and treated sands using dilatancy rate proposed by Zhang and Salgado (2010). Solid arrows indicate the end of the shearing as ε_a=12%

Table 1 Improvement of MICP-treated sands under different confinements

Reference	This study	Lin *et al.* (2015)	Feng and Montoya (2015)
Confining [kPa]	10 / 30 / 50	25 / 50 / 100	100 / 200 / 400
Cohesion [kPa]	0 → 50	0 → 58	0 → 5
Friction [°]	35 → 35	32 → 31	33 → 37

strength changes from cohesion-dominant to friction angle-dominant; additional work is needed to better understand this behavior.

4.2 Dilatancy tendency of MICP-stabilized sand

The stress-dilatancy relationship of untreated and treated sands can be derived from Mohr-Coulomb failure criteria as according the model presented by Zhang and Salgado (2010), as follows

$$d = \frac{9(M-\eta)-3m_c}{9+M(3-2\eta)+m_c} \tag{4}$$

where, d is a dilatancy rate as $\dot{\varepsilon}_v^p/\dot{\varepsilon}_s^p$ ($\dot{\varepsilon}_v^p$: plastic volumetric strain rate, $\dot{\varepsilon}_s^p$: plastic deviatoric strain rate), η is a stress ratio as q/p', M is a stress ratio at critical state defined as η at 12% axial strain in this paper, and m_c is a cohesion factor given by Eq. (5)

$$m_c = \frac{6(3-M)\left(\frac{c}{p'}\right)^2}{3-\eta} - \frac{2c(3-M)}{p'}\sqrt{\left(\frac{\frac{3c}{p'}}{3-\eta}\right)^2 + \frac{3+2\eta}{3-\eta}} \tag{5}$$

The dilatancy-stress ratio relationship is shown in Fig. 13. When the plastic volumetric strain rate is higher than the plastic deviatoric strain rate, d is larger than 1, and vice versa. Data in Fig. 13 show that $\dot{\varepsilon}_v^p$ values of untreated sands are lower than $\dot{\varepsilon}_s^p$; therefore, d is always lower than unity (e.g., -0.1~0.9). When untreated sand reaches the peak stress, the computed dilatancy rates are equal to zero; d values at ε_a=12% are almost zero, and no dilatancy is observed. Therefore, the untreated sands show contractive behavior. Treated sands, however, generally show d=1.4~1.5 at the beginning phase of shearing and decrease until the stress ratio reaches the peak strength. Thereafter, d increases again as the strain increases. As the confinement lowers, the dilatancy rate shows higher for MICP-treated sands. All d values at the peak stress are below 1.0, specifically d = 0.57, 0.05, and 0.2 for the specimens confined at p'_c = 10 kPa, 30 kPa, and 50 kPa, respectively. However, d values at ε_a=12% vary according to the confinement as 1.32, 1.0, and 0.7 for 10 kPa, 30 kPa, and 50 kPa, respectively. It implies that the specimen is highly dilative at small strain, but becomes contractive until the occurrence of the peak stress due to the breakage of the bonding. The softening behavior is observed with increasing strain; however, the dilatancy increases as the specimen densified due to the shearing with drainage. The results show that MICP-treated sands exhibit well defined dilative behavior versus the contractive behavior of untreated sands.

4.3 Debonding of MICP-stabilized sands

Although the calcium carbonate precipitation on the particle surface increases the shear resistance of sand, it is not the main contributor to the improvement of the erodibility resistance. Particle detachment is less affected by the roughness of soils than the bonding between particles (Briaud *et al.* 2017). As addressed in section 4.1, it implies that the improvement of soil's erodibility was mainly achieved by adding a cohesion component.

An alternative precipitation pattern, for example under unsaturated conditions, can potentially provide higher resistance against erosion as the menisci at particle contacts facilitate preferential precipitation at particles contacts rather than on particle surfaces (Cheng *et al.* 2013). Potential scour resistance under unsaturated conditions can be used to strengthening a levee against crown scour due to plunging overtopping floodwater (as occurred during Hurricane Katrina). In addition, the slight change in the hydraulic conductivity observed herein due to MICP facilitates the erodibility improvement because the material remains permeable which allows induced pore pressures to dissipate.

The removal of overburden pressure can cause the calcium carbonate bonds to degrade (Shahin *et al.* 2017). This phenomena has implications for the erodibility assessments, as the sand was cemented under a confinement of 50 kPa (which was then removed for the impinging jet tests). Fig. 7(b) showed that debonding is initiated at approximately 0.1% axial strain as the cementation renders the soils brittle. Therefore, unloading, even at low overburden stress, may lead to particle debonding depending on the level of cementation.

5. Conclusions

Data from this study indicated the MICP process improves the strength and resistance to erosion of sand via bonding the particles with calcium carbonate. The distribution of the calcium carbonate precipitation varied with the level of the improvement. Triaxial testing was conducted at relatively low confining stress, and results indicated that improvement is achieved through the addition of a cohesion component as assessed using the Mohr-Coulomb criterion. Microscopic analysis showed that precipitation takes place at the particle contact points as well as on the particle surfaces. The change in the hydraulic conductivity with the introduction the MICP process under low confining stress are found to be minimal since the cementation is achieved by forming mineral bridges between particle contact points rather than filling the entire voids.

Data from triaxial testing indicated that potential debonding of MICP-treated sand was initiated at a relatively small strain; softening behavior was attributed to the occurrence of such debonding. The treated specimens exhibited more of a dilative behavior compared to the untreated specimens. In this case, the treated sand shows brittle failure with distinct shear bands, while the untreated sands exhibited a ductile failure with a bulging deformation mode. The shear wave velocity was monitored during shearing; its value provided an indication of bond degradation and, therefore, a better understanding of the shear response of the bio-treated soils.

The erodibility of treated sand under submerged impinging jet indicated substantial increase in the critical shear stress and decrease in the erosion rate parameter. Such a trend was observed as a function of level of cementation. These results indicate sufficient potential of MICP for the purpose of erosion and scour mitigation. More testing, however, should be performed to confirm and extend the improvement in erosion characteristics for a wider range of soils and MICP-stabilization protocols.

Acknowledgements

The research described in this paper is financially supported by the state grant from the Renewable Ocean Energy Program for the State of North Carolina through the UNC Coastal Studies Institute (CSI). This work was performed in part at the Analytical Instrumentation Facility (AIF) at North Carolina State University, which is supported by the State of North Carolina and the National Science Foundation (ECCS #1542015). The AIF is a member of the North Carolina Research Triangle Nanotechnology Network (RTNN), a site in the National Nanotechnology Coordinated Infrastructure (NNCI).

References

Al-Madhhachi, A.T., Hanson, G.J., Fox, G.A., Tyagi, A.K. and Bulut, R. (2013), "Measuring soil erodibility using a laboratory "mini" JET", *Trans. ASABE*, **56**(3), 901-910.

Bolton, M.D. (1986), "The strength and dilatancy of sands", *Geotechnique*, **36**(1), 65-78.

Briaud, J.L. (2006), "Bridge scour", *Geotech. News*, **24**(3).

Briaud, J.L. (2013), *Geotechnical Engineering: Unsaturated and Saturated Soils*, John Wiley & Sons.

Briaud, J.L., Govindasamy, A.V. and Shafii, I. (2017), "Erosion charts for selected geomaterials", *J. Geotech. Geoenviron. Eng.*, **143**(10), 04017072.

Cheng, L., Cord-Ruwisch, R. and Shahin, M.A. (2013), "Cementation of sand soil by microbially induced calcite precipitation at various degrees of saturation", *Can. Geotech. J.*, **50**(1), 81-90.

Cheng, L., Shahin, M. and Cord-Ruwisch, R. (2014), "Bio-cementation of sandy soil using microbially induced carbonate precipitation for marine environments", *Géotechnique*, **64**(12), 1010-1013.

Clough, G.W., Sitar, N., Bachus, R.C. and Rad, N.S. (1981), "Cemented sands under static loading", *J. Geotech. Geoenviron. Eng.*, **107**, 799-817.

Dadda, A., Geindreau, C., Emeriault, F., du Roscoat, S.R., Filet, A.E. and Garandet, A. (2018), "Characterization of contact properties in biocemented sand using 3D X-ray micro-tomography", *Acta Geotechnica*, 1-17.

DeJong, J.T., Fritzges, M.B. and Nüsslein, K. (2006), "Microbially induced cementation to control sand response to undrained shear", *J. Geotech. Geoenviron. Eng.*, **132**(11), 1381-1392.

DeJong, J.T., Mortensen, B.M., Martinez, B.C. and Nelson, D.C. (2010), "Bio-mediated soil improvement", *Ecol. Eng.*, **36**(2), 197-210.

Feng, K. and Montoya, B.M. (2015), "Influence of confinement and cementation level on the behavior of microbial-induced calcite precipitated sands under monotonic drained loading", *J. Geotech. Geoenviron. Eng.*, **142**(1), 04015057.

Feng, K., Montoya, B.M. and Evans, T.M. (2017), "Discrete element method simulations of bio-cemented sands", *Comput. Geotech.*, **85**, 139-150.

Ferris, F.G., Phoenix, V., Fujita, Y. and Smith, R.W. (2004), "Kinetics of calcite precipitation induced by ureolytic bacteria at 10 to 20°C in artificial groundwater", *Geochim. Cosmochim. Acta*, **68**(8), 1701-1710.

Garcia-Bengochea, I. and Lovell, C.W. (1981), *Correlative Measurements of Pore Size Distribution and Permeability in Soils*, in *Permeability and Groundwater Contaminant Transport*, ASTM International.

Gomez, M.G., Anderson, C.M., Graddy, C.M., DeJong, J.T., Nelson, D.C. and Ginn, T.R. (2016), "Large-scale comparison of bioaugmentation and biostimulation approaches for biocementation of sands", *J. Geotech. Geoenviron. Eng.*, **143**(5), 04016124.

Hanson, G.J. and Cook, K.R. (2004), "Apparatus, test procedures, and analytical methods to measure soil erodibility in situ", *Appl. Eng. Agricult.*, **20**(4), 455-462.

Jiang, N.J., Soga, K. and Kuo, M. (2016), "Microbially induced carbonate precipitation for seepage-induced internal erosion control in sand-clay mixtures", *J. Geotech. Geoenviron. Eng.*, **143**(3), 04016100.

Khanal, A., Fox, G.A. and Al-Madhhachi, A.T. (2016), "Variability of erodibility parameters from laboratory mini jet erosion tests", *J. Hydrol. Eng.*, **21**(10), 04016030.

Kim, D. and Park, K. (2017), "Evaluation of the grouting in the sandy ground using bio injection material", *Geomech. Eng.*, **12**(5), 739-752.

Lin, H., Suleiman, M.T., Brown, D.G. and Kavazanjian Jr, E. (2015), "Mechanical behavior of sands treated by microbially induced carbonate precipitation", *J. Geotech. Geoenviron. Eng.*, **142**(2), 04015066.

Maleki, M., Ebrahimi, S., Asadzadeh, F. and Tabrizi, M.E. (2016), "Performance of microbial-induced carbonate precipitation on wind erosion control of sandy soil", *Int. J. Environ. Sci. Technol.*, **13**(3), 937-944.

Martinez, B.C., DeJong, J.T. and Ginn, T.R. (2014), "Bio-geochemical reactive transport modeling of microbial induced calcite precipitation to predict the treatment of sand in one-dimensional flow", *Comput. Geotech.*, **58**,1-13.

Montoya, B.M. (2018), "Editorial", *Environ. Geotech.*, **5**(2), 67-68.

Montoya, B.M. and DeJong, J.T. (2015), "Stress-strain behavior of sands cemented by microbially induced calcite precipitation", *J. Geotech. Geoenviron. Eng.*, **141**(6), 04015019.

Montoya, B.M., Gerhard, R., DeJong, J.T., Weil, M., Martinez, B. and Pederson, L. (2012), "Fabrication, operation, and health monitoring of bender elements for aggressive environments", *Geotech. Test. J.*, **35**(5), 28-742.

Nafisi, A., Montoya, B.M. and Evans. T.M. (2019), "Shear strength envelopes of bio-cemented sands with varying particle size and cementation", *J. Geotech. Geoenviron. Eng.*, In Review.

Nassar, M.K., Gurung, D., Bastani, M., Ginn, T.R., Shafei, B., Gomez, M.G., Graddy, C.M., Nelson, D.C. and DeJong, J.T. (2018), "Large-Scale experiments in microbially induced calcite precipitation (MICP): Reactive transport model development and prediction", *Water Resour. Res.*, **54**(1), 480-500.

NBI (National Bridge Inventory) (2016), *Bridge Management Branch*, Federal Highway Administration, Washington, D.C., U.S.A.

NEHRP (National Earthquake Hazards Reduction Program) (2003), *Recommended Provisions for Seismic Regulations for New Buildings and Other Steel Structures. Part 1: Provisions*, Federal Emergency Management Agency, Washington, D.C., U.S.A.

Putra, H., Yasuhara, H., Kinoshita, N. and Hirata, A. (2017), "Application of magnesium to improve uniform distribution of precipitated minerals in 1-m column specimens", *Geomech. Eng.*, **12**(5), 803-813.

Qureshi, M.U., Chang, I. and Al-Sadarani, K. (2017), "Strength and durability characteristics of biopolymer-treated desert sand", *Geomech. Eng.*, **12**(5), 785-801.

Richardson, E.V., Harrison, L.J. and Davis, S.R. (1991), *Evaluating Scour at Bridges*, HEC-18, Report FHWA-IP-90-017, Washington, D.C., U.S.A.

Salifu, E., MacLachlan, E., Iyer, K.R., Knapp, C.W. and Tarantino, A. (2016), "Application of microbially induced calcite precipitation in erosion mitigation and stabilisation of sandy soil foreshore slopes: A preliminary investigation", *Eng. Geol.*, **201**, 96-105.

Shahin, S., Montoya, B.M. and Gabr. M.A. (2017), *Effect of Microbial Induced Calcium Carbonate Precipitation on the Performance of Ponded Coal Ash*, Association of State Dam Safety.

Sidik, W.S., Canakci, H., Kilic, I.H. and Celik, F. (2014), "Applicability of biocementation for organic soil and its effect on permeability", *Geomech. Eng.*, **7**(6), 649-663.

Stocks-Fischer, S., Galinat, J.K., and Bang, S.S. (1999), "Microbiological precipitation of CaCO3", *Soil Biol. Biochem.*, **31**(11), 1563-1571.

van Wijngaarden, W.K., Vermolen, F.J., van Meurs, G.A.M. and Vuik, C. (2011), "Modelling biogrout: A new ground improvement method based on microbial-induced carbonate precipitation", *Transport Porous Med.*, **87**(2), 397-420.

Zhan, Q., Qian, C. and Yi, H. (2016), "Microbial-induced mineralization and cementation of fugitive dust and engineering application", *Construct. Build. Mater.*, **121**, 437-444.

Zhang, J. and Salgado, R. (2010), "Stress-dilatancy relation for Mohr-Coulomb soils following a non-associated flow rule", *Geotechnique*, **60**(3), 223-226.

CC